Parametric analysis of biomass fast pyrolysis in a downer fluidized bed reactor

Accepted Manuscript

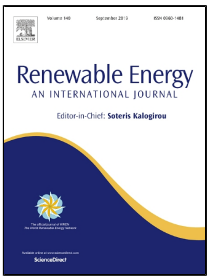

Parametric analysis of biomass fast pyrolysis in a downer fluidized bed reactor

Yassir Makkawi, Xi Yu, Raffaella Ocone

PII:	S0960-1481(19)30750-5
DOI:	10.1016/j.renene.2019.05.077
Reference:	RENE 11669
To appear in:	*Renewable Energy*
Received Date:	08 November 2018
Accepted Date:	17 May 2019

Please cite this article as: Yassir Makkawi, Xi Yu, Raffaella Ocone, Parametric analysis of biomass fast pyrolysis in a downer fluidized bed reactor, *Renewable Energy* (2019), doi: 10.1016/j.renene.2019.05.077

Parametric analysis of biomass fast pyrolysis in a downer fluidized bed reactor

Yassir Makkawi [1,*], Xi Yu[2], Raffaella Ocone[3],

1. Department of Chemical Engineering, American University of Sharjah, P.O. Box 26666, Sharjah, United Arab Emirates

2. European Bioenergy Research Institute (EBRI), School of Engineering and Applied Science, Aston University, Birmingham B4 7ET, United Kingdom

3. *School of Engineering and Physical Sciences, Heriot-Watt University, Edinburgh EH14 4AS, United Kingdom*

Abstract

This study presents a theoretical parametric analysis of biomass fast pyrolysis in a downer reactor, as part of a dual fluidized bed system. The model framework uses a Eulerian-Eulerian CFD approach and incorporates a user-defined function (UDF) for the thermochemical conversion of biomass. The downer reactor consists of a novel gas-solid separator, which is employed to control the gas residence time within the reactor. The parameters investigated included the reactor temperature, the particles (heat carrier and biomass) and the gas residence time. The product yield was found to be strongly dependent on the reactor temperature (varied through changing the heat carrier flow rate), intermediately dependent on the sweeping gas (N_2) flow rate and the sand particle size, and much less dependent on the biomass particle diameter (within the range of 1 mm). The developed model and the results demonstrate the advantage and robustness of employing the model for parameters optimization and sensitivity investigation when dealing with complex multiphase flow reactive system. This conclusion will benefit future development and scale-up studies of downer reactors for biomass fast pyrolysis.

Keywords: Biomass, fast pyrolysis, Eulerian-Eulerian, CFD, downer reactor, parametric analysis.

* Corresponding author: Tel.: +97165152167; fax: +97165152979; E-mail address: ymakkawi@aus.edu (Yassir T. Makkawi).

1. Introduction

The application of fast pyrolysis for the production of biofuels from biomass is currently receiving increasing interest driven by the world growing demand for renewable energies. Fast pyrolysis is a thermochemical process commonly used for the conversion of biomass to liquid fuel (bio-oil). In this process, the biomass is first thermally degraded in an oxygen deficient environment to produce pyrolysis gas and biochar. The bio-oil is then produced following rapid downstream quenching and cooling of the pyrolysis gas.

During the past few decades, the increasing interest in biomass thermal conversion technologies has been matched with considerable progress in reactors design and optimization. The most widely studied reactors for pyrolysis and general biomass thermal conversion are the fluidized and fixed bed reactors. Reviews on the operating principles and advantages/disadvantages of the various types of fast pyrolysis reactors are available in the literature (e.g. Lede [1], Bridgwater [2]). The focus of this study is on a downer reactor (also referred to as drop tube, free-fall and concurrent fluidized bed). Theoretical and experimental studies of biomass pyrolysis in a downer reactor are generally rare. The authors are not aware of any reported theoretical studies fully devoted to the parametric analysis of this type of reactor, with the exception of the study by the authors, which was focused on the hydrodynamic aspects of the reactor (Yu et al. [3]). This is despite its distinct advantages, such as uniformity in gas and solids flow structure compared to up-flow (circulating and bubbling) and fixed bed reactors (Zhu et al. [4]). In addition to that, downer reactors are known to be simple in design, easier to operate and control the gas-solid contact time. The latter is a desirable feature in biomass fast pyrolysis in order to control the product quality. In a simple description, in a conventional downer reactor, the biomass undergoes rapid thermal degradation while freely falling inside a hot chamber. In order to create a positive pressure at the entrance and allow sweeping of the pyrolysis gas, an inert gas, such as nitrogen, is usually introduced at the top. The produced biochar and pyrolysis gas are collected at the bottom of the reactor, where the latter is rapidly cooled to produce bio-oil and non-condensable gas. The pyrolysis downer reactor can be operated in a single mode or integrated within a closed loop to create what is usually referred to as twin or dual circulating fluidized bed (DCFB) system (see the illustrative diagrams in Fig. 1). In the former case, combustion of a primary biomass feed is used to satisfy the endothermic pyrolysis reaction of a secondary biomass feed, while in the latter case the process is sustained by heat supplied from the combustion of the by-product biochar in a second reactor. In this study, the focus is on the downer pyrolysis reactor as part of a DCFB in Fig. 1-b.

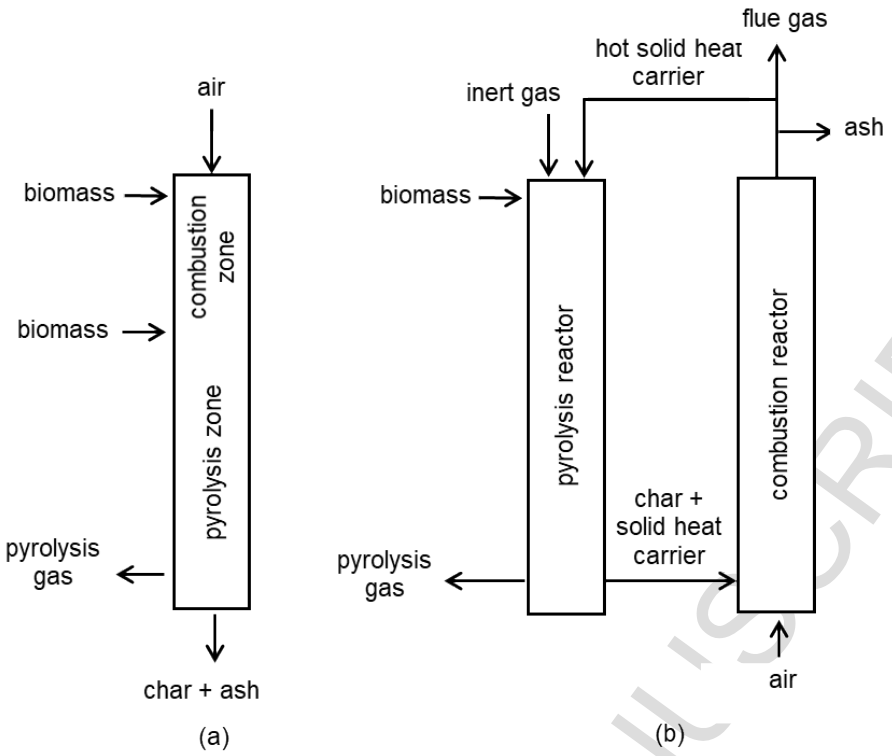

Fig. 1. Examples of the configuration of sustainable biomass pyrolysis reactors without the reliance on external heating (a) single mode fluidized bed (b) twin or dual circulating fluidized bed (DCFB) system.

In pyrolysis experiments, measurement of the process response to the variations of the operating conditions is usually challenging due to the limitation imposed by the nature of the process, i.e. high temperature and release of hydrocarbon gases. Computational fluid dynamic (CFD) offers the option for conducting comprehensive parametric analysis at a low cost with the added advantages of providing detailed localized data (e.g. flow hydrodynamics, temperature and chemical reactions) at a wide range of operating parameters. The use of CFD in the analysis of reactive and non-reactive multiphase flow system has been recently reported in a number of recent publications (e.g. Bashir et al.[5], Elewuwa and Makkawi, [6], Yu et al. [7], Hassan and Makkawi [8]). Of direct relevance to this study is the series of papers by Yu et al. [3, 7] in which a Eulerian–Eulerian CFD model was developed and validated for the prediction of biomass pyrolysis in a downer pyrolysis reactor. The model proved to be highly useful in predicting the details of the flow hydrodynamics and thermochemical behavior in fluidized bed reactors.

In biomass pyrolysis, the reaction temperature and the gas residence time are the two most important parameters to control during the process. Both parameters have been widely reported to dictate the distribution of the final product (biochar, bio-oil and permanent gas) (Bridgwater [2], Bridgwater [9]). It is therefore important when designing and operating a pyrolysis reactor, to keep in mind the relation between the desired quantity/quality of the products and the reactor operating temperature and gas residence time. The reactor operating temperature is commonly reported in the parametric analysis of biomass pyrolysis. Its effect is interrelated with other process parameters, such as the gas residence time and the rate of heat transfer between the gas and solid phases inside the reactor. For the same type of reactor, the difference in optimum pyrolysis temperature is mainly due to the variations in the biomass content of lignin, cellulose, and hemicellulose. Each of these key constituents of biomass decomposes at a different range of temperature (Lin et al. [10]). The majority of studies have shown a maximum bio-oil yield at an optimum pyrolysis temperature within the range of 400−900 ºC. Bridgwater [9] Suggested a reaction temperature of around 500 ◦C is ideal for maximizing bio-oil yield. In an experimental study by Yu et al. [11], the bio-oil produced from birch wood pyrolysis in a free fall reactor was found to be maximum at the temperature of 700 ºC. In another experiment, investigating the pyrolysis of pine wood in a bubbling fluidized bed, Westerhof et al. [12] have shown that the pyrolysis gas yield increases steadily with increasing temperature from 450 to 580 °C then decreases beyond that.

The effect of gas residence time is frequently investigated by changing the flow rate of the sweeping or carrier gas (e.g. Gerçel [13], Gabel [14], Ellens [15]). The sweeping gas (commonly nitrogen) is used to create an oxygen free environment and control the residence time of the pyrolysis gas inside the hot zone of the reactor, as noted earlier. Additionally, in fluidized bed reactors, the sweeping gas serves as a fluidizing medium to promote mixing and enhances the heat and mass transfer. The sweeping gas flow rate has also a strong effect on the particle/gas residence time, rate of heating and general flow structure. The gas residence time can be controlled by increasing or decreasing the sweeping gas flow rate. Short residence time help in limiting the gas thermal and catalytic cracking during gas-char contact, hence, increasing the bio-oil yield. In one of the very few studies on experimental parametric analysis of a free fall reactor, Ellens [15] recommended to maintaining the sweeping gas flow rate in order to achieve adequate pyrolysis. Gable [14] showed a slightly positive impact of increasing sweeping gas on the pyrolysis yield. A similar conclusion was reached by Onay and Koçkar

[16] who observed that little gain in the bio-oil yields was achieved in a free fall pyrolysis reactor when increasing the sweep gas flow rates beyond 50 mL/min.

Other parameters that have been reported to affect the pyrolysis products and the overall reactor performance are the biomass and heat carrier (sand) particle sizes (e.g. Shen et al. [17], Liu et al. [18]). Biomass generally has a low thermal conductivity; therefore, it is important to use a finely ground biomass in order to limit the particle internal thermal resistance (Bridgwater [2]). Uzun et al. [19] experimentally investigated the effect of the biomass particle size on the bio-oil yield using a fixed bed reactor at a pyrolysis temperature of 500 C. It was shown that the optimum biomass particle size for maximum bio-oil yield is within the range of 0.425 mm< d_p < 0.85 mm. Within this range, negligible variation in the overall process yield and product distribution was observed. In agreement with this, Jahirul et al. [20] suggested using biomass particle size <1 mm. For a biomass particle within this size range and undergoing pyrolysis at the temperature range of 500 ºC the estimated Biot number falls below unity. It is for this reason that the heat transfer mechanism and release of volatiles at the single particle level remains independent of the biomass and of the heat carrier particle size as long as the d_p falls below 1.0 mm. Nevertheless, one should not ignore the important role that particle size plays in identifying the overall hydrodynamics, such as the solid distribution and the solid velocity.

2. Process description and objectives of the study

The pyrolysis reactor and the simulation domain considered in this study are shown in Fig. 2. In this arrangement, the biomass and sand enter the reactor from the top and concurrently flow towards the bottom under the influence of gravity and drag force exerted by the carrier gas nitrogen. The sand, which enters at the reactor at a high temperature, is assumed to drive the endothermic pyrolysis process. At the bottom of the reactor, sand and char are collected in a receiving tank while the gas is discharged through a pipe inserted under a solid-gas separator. This separation mechanism, which is specifically designed for downer pyrolysis reactors by researchers at the ICFAR in Canada [21], has been experimentally tested and numerically studied by Yu et a. [7] and Huard et al. [22].

The focus of the present parametric study is to elucidate the thermochemical behavior of the process and the impact of the process parameters on the pyrolysis product yield and distribution. The specific objectives are:

1. To examine the reactor sensitivity and impact of the following parameters on the pyrolysis

product yield and overall reactor performance:

i. Reactor temperature varied through manipulating the flow rate of the heat carrier material (sand).
ii. Gas residence time varied through manipulating the flow rate of the carrier gas (nitrogen).
iii. Biomass and heat carrier (sand) varied through manipulating the particle sizes.

2. To demonstrate the advantage and robustness of the developed CFD model for the parametric analysis of pyrolysis reactors.

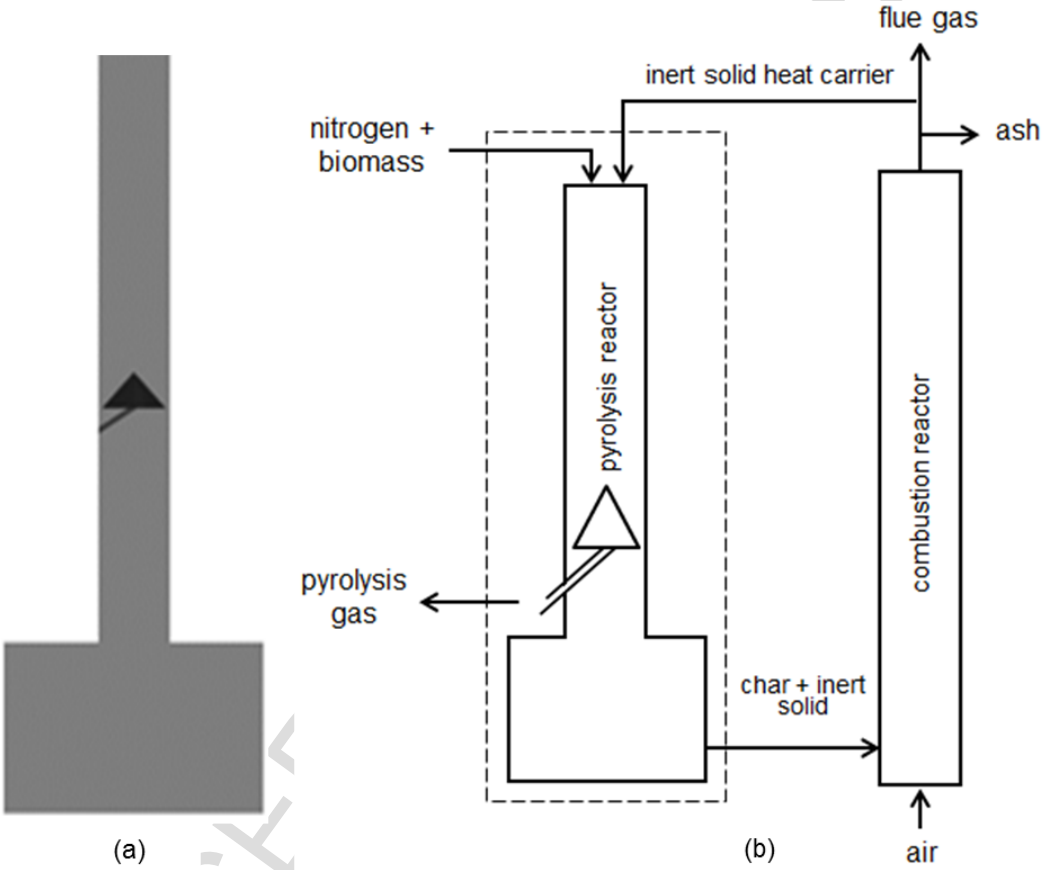

Fig. 2. Schematic representation of (a) the pyrolysis reactor simulation domain, and (b) the overall closed loop pyrolysis process with the simulation domain inside the dotted box.

3. Model equations

The Eulerian-Eulerian CFD model reported by Yu el al. [3, 7] for the simulation of biomass pyrolysis in a downer reactor has been used to carry out this parametric analysis. The model is solved in three-dimensional coordinates using ANSYS-FLUENT CFD code. The multiphase flow inside the reactor is assumed to consist of two solid phases (sand and biomass) and one

gas phase consisting of various species, namely, a condensable fraction (bio-oil) and a non-condensable fraction consisting of CO, CO_2, CH_4, H_2 and H_2O. The main equations describing the hydrodynamics, heat transfer and reaction are given below. The full model, including detailed constitutive relations and a user-defined function (UDF) for the pyrolysis reaction, can be found in Yu et al. [3, 7].

3.1. Continuity, momentum and granular energy equations

The gas and solids phases continuity equation are given by:

$$\frac{\partial(\alpha_g\rho_g)}{\partial t}+\nabla(\alpha_g\rho_g\vec{u}_g)=R_g \quad (1)$$

$$\frac{\partial(\alpha_{s_i}\rho_{s_i})}{\partial t}+\nabla(\alpha_{s_i}\rho_{s_i}\vec{u}_{s_i})=R_{s_i} \qquad i=1 \text{ or } 2 \quad (2)$$

$$\sum_{i=1}^{2}\alpha_{s_i}+\alpha_g=1 \quad (3)$$

where α is the volume fraction, ρ is the density. $\vec{u}$ is the velocity vector, R is the interphase mass transfer due to biomass pyrolysis and drying. The subscript g, s_1 and s_2 stand for gas, sand and biomass phases respectively. Note that, $R_{s_1}=0$ for the inert solid (sand).

The gas and solids momentum equations are given by:

$$\frac{\partial(\alpha_g\rho_g\vec{u}_g)}{\partial t}+\nabla(\alpha_g\rho_g\vec{u}_g\vec{u}_g)=-\alpha_g\nabla P+\nabla\bar{\tau}_g - \sum_{i=1}^{2}\beta_{gs_i}(\vec{u}_g-\vec{u}_{s_i})+\alpha_g\rho_g\vec{g}+\vec{R}_{s_2g}+\dot{m}_{s_2g}\vec{u}_{s_2g} \quad (4)$$

$$\frac{\partial(\alpha_{s_1}\rho_{s_1}\vec{u}_{s_1})}{\partial t}+\nabla(\alpha_{s_1}\rho_{s_1}\vec{u}_{s_1}\vec{u}_{s_1}) =-\alpha_{s_1}\nabla P-\nabla P_{s_1}+\nabla\bar{\tau}_{s_1}+\beta_{gs_1}(\vec{u}_g-\vec{u}_{s_1})+\beta_{s_1s_2}(\vec{u}_{s_2}-\vec{u}_{s_1})+\alpha_{s_1}\rho_{s_1}\vec{g} \quad (5)$$

$$\frac{\partial(\alpha_{s_2}\rho_{s_2}\vec{u}_{s_2})}{\partial t}+\nabla(\alpha_{s_2}\rho_{s_2}\vec{u}_{s_2}\vec{u}_{s_2}) =-\alpha_{s_2}\nabla P-\nabla P_{s_2}+\nabla\bar{\tau}_{s_2}+\beta_{gs_2}(\vec{u}_g-\vec{u}_{s_2})+\beta_{s_2s_1}(\vec{u}_{s_1}-\vec{u}_{s_2})+\alpha_{s_2}\rho_{s_2}\vec{g}+\vec{R}_{gs_2}-\dot{m}_{s_2g}\vec{u}_{s_2g} \quad (6)$$

where β_{gs} and β_{ss} are the gas-solid and solid-solid momentum exchange coefficients, respectively, $\vec{g}$ is the gravity constant, $\bar{\tau}$ is the solid shear stress tensor, $\vec{R}$ is the interphase momentum transfer due to the pyrolysis reaction, and $\dot{m}\vec{u}$ is the interphase momentum transfer

due to evaporation. Note that $\vec{R}$ and $\dot{m}\vec{u}$ are not included in Eq. 5, due to the inert nature of the sand particles.

The granular energy equation is given by:

$$\frac{3}{2}\left[\frac{\partial(\alpha_{s_i}\rho_s\Theta_{s_i})}{\partial t}+\nabla(\alpha_{s_i}\rho_s\Theta_{s_i})\vec{u}_{s_i}\right]= \left(-P_{s_i}\bar{I}+\bar{\tau}_{s_i}\right):\nabla\vec{u}_{s_i}+\nabla\left(\kappa_{\Theta_{s_i}}\nabla\Theta_{s_i}\right)-\gamma_{\Theta_{s_i}}+\sum_{k=1}^{2}\phi_{ks_i} \quad (7)$$

where Θ_s is the pseud-granular temperature of solid phase, κ_{Θ_s} is diffusion coefficient of granular energy, and ϕ_{ks} is energy exchange between phase k and solid phase.

Note that, in modeling the solid phases it is assumed that the particles are spherical and the biomass particle retains its original size during pyrolysis (i.e. no shrinkage). This simplification is made due to the recognized shortcomings of the classic Eulerian-Eulerian method which lacks the reliable formulation to incorporate the particle shrinkage associated with particle drying and pyrolysis.

3.2. Pyrolysis reaction and drying models

The biomass is treated as a solid phase consisting of volatile matters, fixed carbon, ash and water. The composition of the biomass, which is assumed to match that of a switchgrass, is given in Table 1. The pyrolysis is described by one-global reaction scheme as follow (Boateng and Mtui [23], Yu et al. [7], Bashir et al. [5]):

$$Biomass \rightarrow 0.138\ char + 0.805\ biooil + 0.15\ H_2O + 0.003\ H_2 + 0.035\ CO + 0.018\ CO_2 + 0.008\ CH_4 \quad (8)$$

According to Eq. (8) the overall non-condensable gas (NCG) is assumed to consist of H_2, CO, CO_2 and CH_4, with the distribution as per the given coefficients. The rate of the pyrolysis reaction is given by the following formula, specifically derived for switch grass pyrolysis as follows (Pasangulapati [24]):

$$r=\left[2.16\times10^{7}exp\left(\frac{-1.037\times10^{7}}{RT}\right)\right]\alpha_{s_2}\ [C_{vol}]^{0.67} \quad (9)$$

Note that in the above model the homogeneous reactions (between the pyrolysis gas species) and heterogeneous catalytic reactions between the gas and char are ignored. This is a reasonable

assumption since the employed gas-solid separation mechanism allows for limiting the contact between the pyrolysis gas and char while maintaining the gas residence time at the desired range of < 2 s (Yu et al. [7]).

Table 1. Chemical composition of switch grass (Boateng et al. [25])

	Fixed carbon	Moisture	Volatile	Ash
Proximate analysis (wt%)	13.81	2.65	81.20	2.54
	C	H	O	N
Ultimate analysis (wt%)	48.8	6.99	43.68	0.53

The biomass drying was incorporated in the model based on evaporative mass transfer process where the biomass water content is assumed to be converted to moisture and added to the gas phase according to the following mass transfer relation (ANSYS Fluent documentation [26]):

$$\dot{m}_{lv} = k_m \times \alpha_l \rho_l \frac{(T_l - T_{sat})}{T_{sat}} \quad (10)$$

where $\dot{m}_{lv}$ is the mass transfer rate from the liquid phase to the vapur phase per unit volume, $k_m = 0.1\ s^{-1}$ is the mass transfer coefficient, α_l and ρ_l represent the moisture volume fraction and density, respectively, T_l is the gaseous phase temperature and T_{sat} is the saturation temperature taken as 100 °C.

3.3. Heat balance

The heat balance equation for the gas and solid phases are given by:

$$\frac{\partial(\alpha_g \rho_g h_g)}{\partial t} + \nabla(\alpha_g \rho_g \vec{u}_g h_g) = \alpha_g \frac{\partial P_g}{\partial t} + \bar{\bar{\tau}}_g : \nabla \vec{u}_g - \vec{q}_g + S_g + Q_{gs_1} + Q_{gs_2} + (\dot{m}_{s_2 g} h_{s_2 g} - \dot{m}_{g s_2} h_{g s_2}) \quad (11)$$

$$\frac{\partial(\alpha_{s_1} \rho_{s_1} h_{s_1})}{\partial t} + \nabla(\alpha_{s_1} \rho_{s_1} \vec{u}_{s_1} h_{s_1}) = \alpha_{s_1} \frac{\partial P_{s_1}}{\partial t} + \bar{\bar{\tau}}_{s_1} : \nabla \vec{u}_{s_1} - \vec{q}_{s_1} + Q_{s_1 g} \quad (12)$$

$$\frac{\partial(\alpha_{s_2} \rho_{s_2} h_{s_2})}{\partial t} + \nabla(\alpha_{s_2} \rho_{s_2} \vec{u}_{s_2} h_{s_2}) = \alpha_{s_2} \frac{\partial P_{s_2}}{\partial t} + \bar{\bar{\tau}}_{s_2} : \nabla \vec{u}_{s_2} - \vec{q}_{s_2} - S_g + Q_{s_2 g} + (\dot{m}_{g s_2} h_{g s_2} - \dot{m}_{s_2 g} h_{s_2 g}) \quad (13)$$

where h_g is the specific enthalpy of the gas phase, $\vec{q}$ is the heat flux, S is a source term that includes the enthalpy due to the chemical reaction, Q is the intensity of the heat exchange between the gas and solid phases. The last term on the right-hand side represents the interphase

enthalpy exchange due to evaporation. Note that, in the above heat balance, the internal thermal resistance at the single particle level is neglected due to the low Biot numbers for both the solid phases (sand and biomass particles).

4. Model solution procedure and boundary conditions

The model equations are solved using finite volume approach. First-order discretization schemes were used for the solution of the convection terms in all governing equations. The relative error between any two successive iterations was specified by using a convergence criterion of 10^{-3} for each scaled residual component. The phase-coupled SIMPLE algorithm (Vasquez and Ivanov [27]) was applied for the pressure-velocity coupling. The linearized governing equations were solved using the block algebraic multi-grid method. In order to avoid numerical instabilities and to ensure that the fast biomass conversion and heat transfer are captured, the solution time step for the reactive system was set to a relatively smaller time step of 0.0005 s for the first 0.5 s then increased to 0.001 s for the rest of the simulation time. The mesh was generated with hybrid cells of structured and unstructured grids, giving a total of 30,785 cells. In order to capture the steep hydrodynamic variations around the walls of the separation device (the conical deflector and the gas exit pipe), the grid size was refined by setting the minimum and maximum grid size at 0.3 and 1.0 cm, respectively. In the remaining of the simulation domain, the minimum and maximum grid size were set at 1.0 and 5.0 cm. respectively. Summary of the reactor dimensions, default operating conditions and simulation parameters are given in Table 2.

Table 2. Summary of the reactor dimensions and the defaults operating conditions

Reactor dimensions*			
Reactor height [m]	1.335	Diameter of the gas exit pipe [cm]	0.95
Reactor diameter [m]	0.069	Position of gas exit from top [cm]	98.6
Default operating parameters			
Pressure outlet [pa]	101,3	Biomass inlet temperature [°C]	25.0
Biomass flow rate [g/s]	5.0	N_2 inlet temperature [°C]	25.0
Nitrogen flow rate [lit/s]	0.187	Sand inlet temperature [°C]	700.0
Sand flow rate [g s^{-1}]	80.0	Sand particle size [mμ]	200.0
Sand density [kg m^{-3}]	2650	Biomass particle size [mμ]	500
Simulation parameters			
Wall-particle restitution coef. [-]	0.8	Maximum solid packing [-]	0.63
Particle-particle restitution coef. [-]	0.9	Specularity coefficient [-]	0.5

Solution convergence criterion (-)	10^{-3}	Maximum number of iterations [-]	20

** Further details on the reactor and separator geometry are available in Yu et al. 2014 [3]*

Table 3. shows the summary of the parameters varied in this study, taking into consideration the effect of the heat carrier (sand) flow rate, particles sizes (sand and biomass) and sweeping gas (nitrogen) flow rate on the pyrolysis products distribution. In total, this makes nine different simulation conditions, including the default setting of Case No 1.

Table 3. Set of the operating conditions considered in the parametric analysis

Parameter	Default	Parameters varied							
		N_2 flow		Sand flow		Particle size			
						Biomass		Sand	
Case No	1	2	3	4	5	6	7	8	9
N_2 flow rate [m^3/h]	0.67	**0.34**	**6.73**	0.67	0.67	0.67	0.67	0.67	0.67
Sand flow [g/s]	80	80	80	**50**	**100**	80	80	80	80
Biomass size [µm]	500	500	500	500	500	**200**	**350**	500	500
Sand size [µm]	200	200	200	200	200	200	200	**350**	**500**

5. Parametric analysis and discussion

5.1. Effect of the reactor temperature

The reactor temperature was varied by varying the heat carrier (sand) flow rate. The choice is made here to vary the sand flow rate because this resembles largely the effects caused by varying the sand temperature with the added advantage of providing the necessary data to assess the associated change in flow hydrodynamics. The range of sand flow rate considered in the analysis was selected based on the following simple energy balance equation:

$$Q_{in} = \sum m\Delta H^{\circ}_{f,298,feed} + \sum m\Delta H_{feed}(T) - \sum n\Delta H^{\circ}_{f,298,prod} - \sum n\Delta H_{prod}(T) \quad (14)$$

where $\Delta H^{\circ}_{f,298,feed}$ and $\Delta H^{\circ}_{f,298,prod}$ are the heats of formation of feed and product materials at temperature 298K per kg material; $H_{feed}(T)$ and $H_{prod}(T)$ are the enthalpies of the feed and products at temperature T (pyrolysis temperature). Using the above equation, the estimated heat input required to derive the pyrolysis of 5 g/s biomass flow is 9.3 KW. For sand entering at 700 ºC and assuming an average reactor temperature of 500 ºC, this heat corresponds to sand flow of around 80 g/s. Therefore, to assess the sensitivity of the downer reactor to the operating temperature, three different sand flow rates of 50, 80 and 100 g/s has been considered. Note that this corresponds to 10−20 times the biomass feed rate, which is within the rule of thumb for thermal conversion of biomass in fluidized bed reactors.

Fig. 3 shows the profiles and contours of the biomass phase temperature at three different sand flow rates of 50 g/s, 80 g/s and 100 g/s. As expected, the increase in the heat carrier flow rate has a direct impact on the reactor temperature, as well as on the overall flow hydrodynamics. In Fig. 3a,b, the profile and contour show that the gas temperature increases sharply from 25 ℃ to above 600 ℃ within a very short entrance length due to the rapid heat transfer from the hot sand (heat carrier) to the gas and biomass phases. The temperature then gradually decrease but with a much lesser extent beyond the lower part of the reactor. The drop in the gas temperature is due to the heat being consumed by drying and pyrolysis of the biomass. The contours of the biomass temperature, shown in Fig. 3c, depicts a different behavior where it is observed that the biomass temperature gradually increases from the entrance temperature of 25 ℃ to reach a peak within the upper part of the reactor. The temperature then remains relatively uniform and stead within most of the lower part of the reactor. Generally, it is observed that the "thermal entrance length" slightly increases with increasing the heat carrier flow rate, which is expected, since this increases the heat supply.

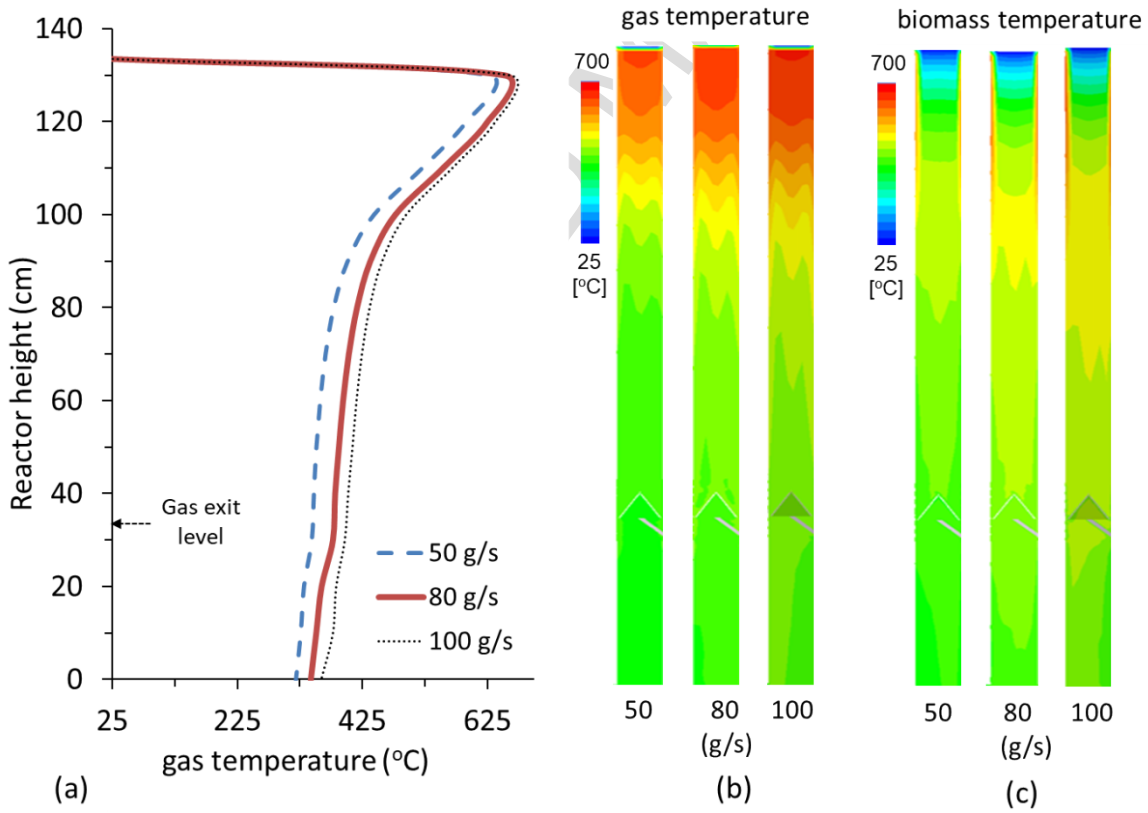

Fig. 3. Variations in the gas and biomass temperatures at various sand flow rates (50−100 g/s) (a) cross-sectional average vertical profile of biomass temperature (b) and (c) contours of the biomass and gas temperatures, respectively.

Fig 4 shows the vertical profile of devolatilization efficiency and contours of the devolatilization rate at the three different sand flow rates considered. The efficiency was calculate cumulatively using the following formula:

$$\eta_{dev} = \frac{m_{volatile} \text{ removed from biomass}}{m_{volatile} \text{ in the biomass feed}} \quad (15)$$

Fig. 4a shows that the cumulative devolatilization efficiency curves consistently shift to the right as the sand flow rate is increased from 50 g/s to 100 g/s. In Fig. 4b, it is generally observed that the devolatilization rate is nearly zero within the thermal entrance length. This is not surprising since this is the region where the biomass and carrier nitrogen undergo rapid convective heating by the hot sand. The devolatilization then commences shortly after that, as indicated in the contours plots. Beyond the gas exit pipe, the devolatilization rate sharply decreases mainly due to the drop in temperature. At this stage, the biomass is converted to the final product of pyrolysis gas and char.

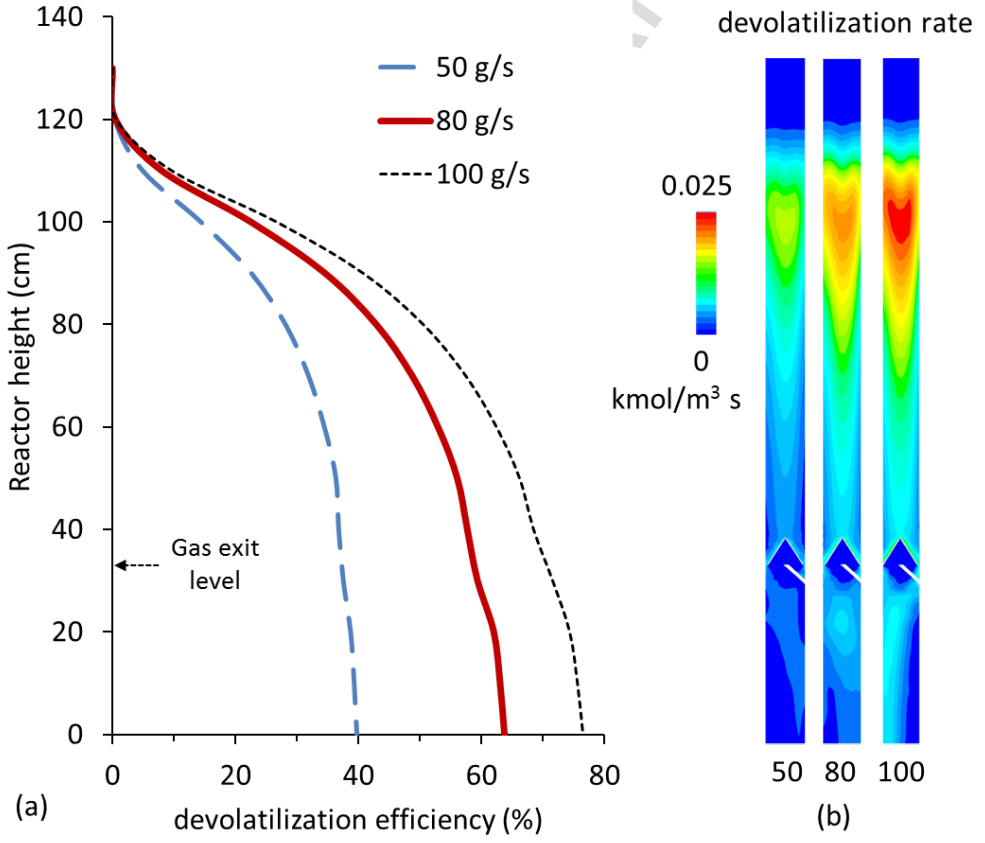

Fig. 4. Biomass devolatilization at steady condition for different heat carrier (sand) flow rates (a) variations of the devolatilization efficiency along the reactor height (b) contours of devolatilization rate.

Fig. 5 shows the temporal evolution of the pyrolysis gas flow and the final product distribution at different sand flow rates. The products consist of liquid bio-oil including water, non-condensable gas (NCG) and char. Fig. 5a shows that the flow of the pyrolysis gas reaches the steady state after ~2 s from the start of the operation. The results also suggest that the flow of the pyrolysis gas increases linearly with increasing the sand flow rate. The data in Fig. 5b shows the bio-oil and NCG to increase with increasing the heat carrier flow, which comes at the expense of decreasing the char yield. This is in agreement with the vast majority of published literature (e.g. Demirbas, 2004 [28]), since increasing the reactor temperature tends to convert the biomass to higher fraction pyrolysis gas with lower biochar production. It should be noted that excessive increase in the reactor temperature, beyond the critical temperature of ~ 600 ºC shifts the pyrolysis process towards the gasification model as the volatiles get thermally cracked to light hydrocarbons, while the char is constituted predominantly by ash and fixed carbon. In the current model, thermal cracking, as well as the reaction between the biochar and gas, are omitted because the temperature remains within the recommended limit and the gas residence time within the hot zone of the reactor is short, as demonstrated in the following section. Quantitatively, the calculation shows that as the temperature is increased by doubling the sand flow (from 50 to 100 g/s), the bio-oil yield and the NCG both increased by 118% and 124%, respectively, which is significantly high.

5.2. Effect of biomass and sand particle sizes

The reaction rate in pyrolysis is widely understood to be strongly dominated by the heat transfer at the particle level. However, the current Eulerian-Eulerian model treats the solid as a continuum phase; hence, the internal thermal resistance, at the single particle level is not incorporated. This is a valid approximation if the particle Biot number is below unity. Here, the Biot number is calculated as follows:

$$Bi = \frac{d_c h}{k} \tag{16}$$

where d_c is a characteristic length [m], h is the convective heat transfer coefficient [W m^{-2} K^{-1}] and k is the thermal conductivity of the particle [Wm^{-1}K^{-1}]. Assuming an average pyrolysis temperature of 500 °C, heat transfer coefficient of 0.65 kW m^{-2} K^{-1}, and thermal conductivity of 0.25 and 0.1 Wm^{-1}K^{-1} for sand and biomass particles respectively, the calculated Biot number was found to fall below unity, hence the approximation employed is valid, as noted earlier. There is also experimental evidence, such as that reported by Seebauer et al., (1979)

[29] and Septien (2012) [30], which indicates that the effect of the particle size on the pyrolysis yield is negligible as long as the size falls below 1.5 mm. The solid-solid conductive heat transfer is also ignored in the current model due to the very low solid concentration. This implies that the change in the particle size would only affect the overall rate of pyrolysis through changing the flow hydrodynamics and the particle surface area available for heat and mass transfer.

Fig. 6 shows the distribution of the biomass solid phase at three different particle sizes (200, 350 and 500 μm) and the corresponding pyrolysis product distribution. Note that the colour code in the contours has been restricted to allow better visualization of the solid concentration variations. In Fig. 6a, it is generally observed that the biomass concertation is high at the entrance and to a lesser extent below the gas exit at the separator. It is also clear that the effect of changing the particle size is limited, consequently, there is a limited impact of this parameter on product distribution, as shown in Fig 6b. This is expected since the biomass flow rate is too low to cause a significant impact on the reactor hydrodynamics. On the contrary, the effect of changing the sand particle size on the flow hydrodynamics and products is well-pronounced, as shown in Fig. 7. Note that the sand flow rate is at least 10 times higher than that of the biomass. In Fig, 7a, the overall flow structure appears to be completely re-shaped at increasing sand flow by forming a highly dense core and dilute walls. This appears to have a positive impact on the bio-oil and NCG gas yields, as shown in Fig. 7b. The decrease in sand particle size, from 500 μm to 200 μm, resulted in increasing the bio-oil and the NCG yields by ~30%, at the expense of a decrease in the char yield. This could also be attributed to the fact that, smaller particles offer higher surface area, hence, higher heat and mass transfer between the various phases. This, in turn, enhances the overall rate of release of pyrolysis gas.

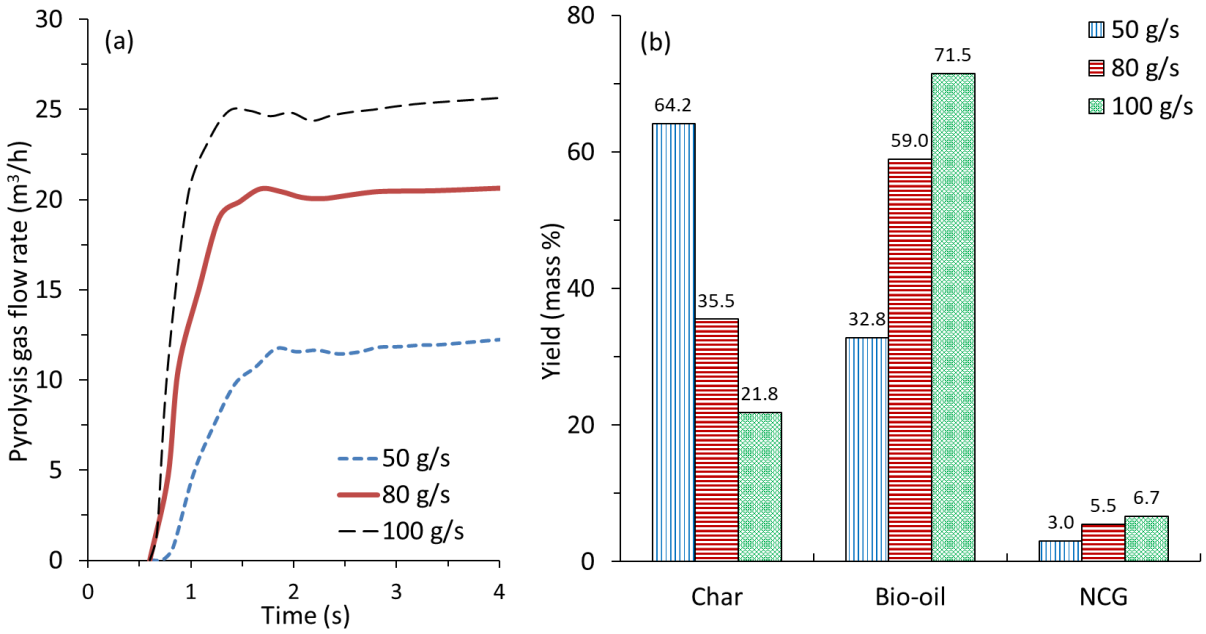

Fig. 5. Effect of the heat carrier flow rate (sand) on the release of pyrolysis gas and product composition (a) Temporal evolution of the pyrolysis gas flow rate at the gas exit pipe, and (b) the corresponding product distribution at different sand (heat carrier) flow rates.

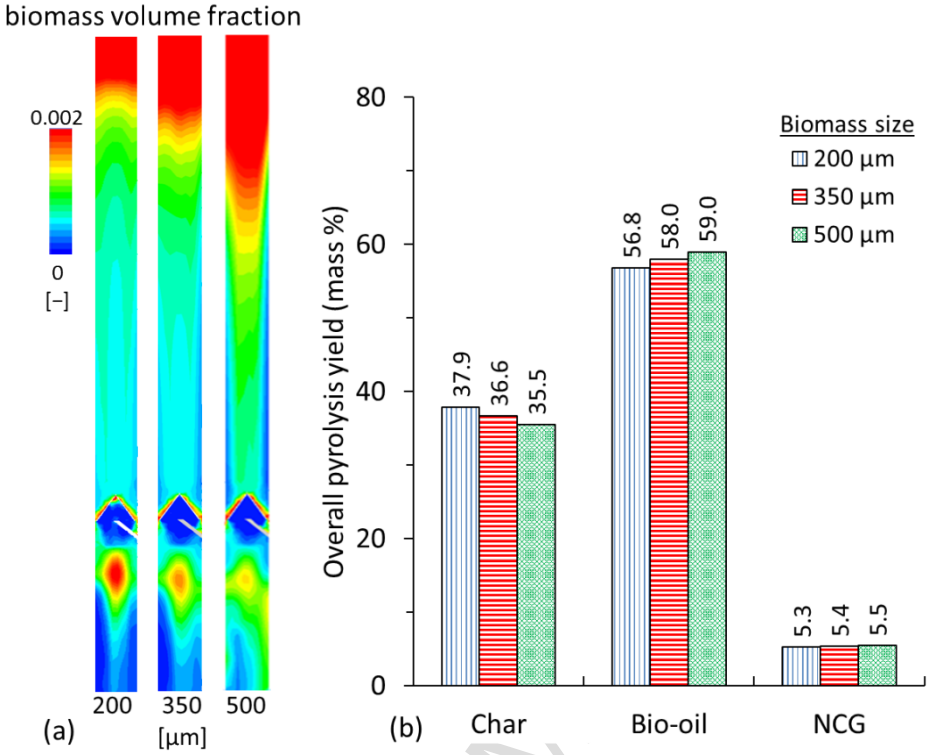

Fig. 6. Effect of the biomass particle size (200−500 µm) on (a) the biomass concentration, and (b) the pyrolysis products distribution.

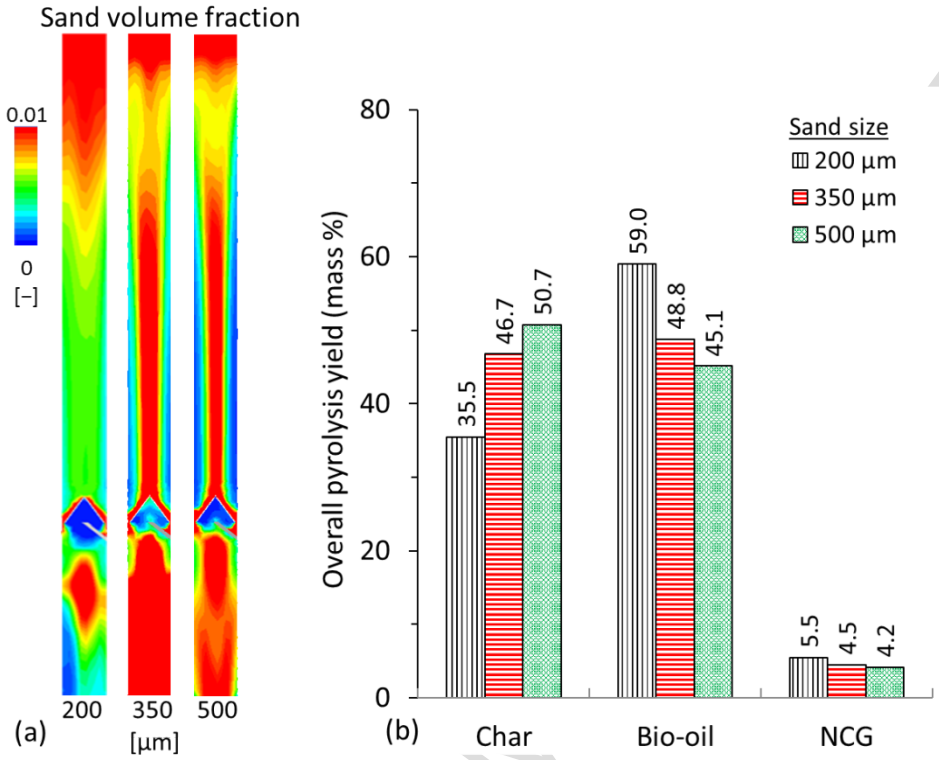

Fig. 7. Effect of the sand particle size on (a) the sand concentration, and (b) the pyrolysis products distribution.

5.3. Effect of nitrogen flow rate

Inert gases, such as nitrogen, helium and argon, are commonly used in biomass fast pyrolysis in order to (i) create an oxygen-free environment (ii) allow sweeping of the produced pyrolysis gas, and, most importantly, (iii) control the gas and solid residence time within the hot reaction zone. In this study, the effect of nitrogen flow was studied using three different flow rates; two within the low flow range (0.34 m^3/h and 0.67 m^3/h) and one excessively high (6.73 m^3/h). The flow rates correspond to nitrogen inlet velocities of 0.025 m/s, 0.05 m/s and 0.5 m/s, respectively. All the other operating parameters were set at the default values, as given in Table 2. In order to relate the applied gas flow to the drag force exerted on particles, the following force balance for a particle in suspension (Makkawi [31]) has been used:

$$F_d = \frac{\pi}{8} d_p^2 \rho_f (u_g)^2 C_d \quad (17)$$

where

$$C_d = 3.0 + 303 e^{-0.135 Re_p} \quad (18)$$

Applying Eqs. 17 and 18 for a biomass particle of 500 μm diameter, the ratio of the gas drag force to the particle weight force (F_d/W) at the nitrogen velocities of 0.025 m/s, 0.05 m/s and 0.5 m/s would be 0.07, 0.23 and 3.13, respectively. In the next paragraphs, it is shown that the ratio F_d/W is of significance for the relation between the gas flow rate, gas residence and the particle weigh force with the pyrolysis yield.

Fig. 8 shows the effect of the nitrogen flow rate on the distribution of the gas residence time (time taken from the inlet to the gas exit pipe). The residence time distribution was obtained based on particle tracking and path lines analysis method [Ghirelli et al. [32]]. It is shown that at the highest nitrogen flow rate the gas residence time distribution is narrowed within the range of 0.3–1.3 s and peaks at ~0.5 s, while at the lowest nitrogen flow, the residence time is widely distributed within the range of 0.5–4 s with a peak at 2 s. In between, at the nitrogen velocity of 0.05 m/s, the residence time distribution is within the range of 0.7–2.7 s and peaks at ~1.5 s, which is close to the range recommended for maximum bio-oil yield by fast pyrolysis (1−2 s) (Bridgwater and Peacoke [33]).

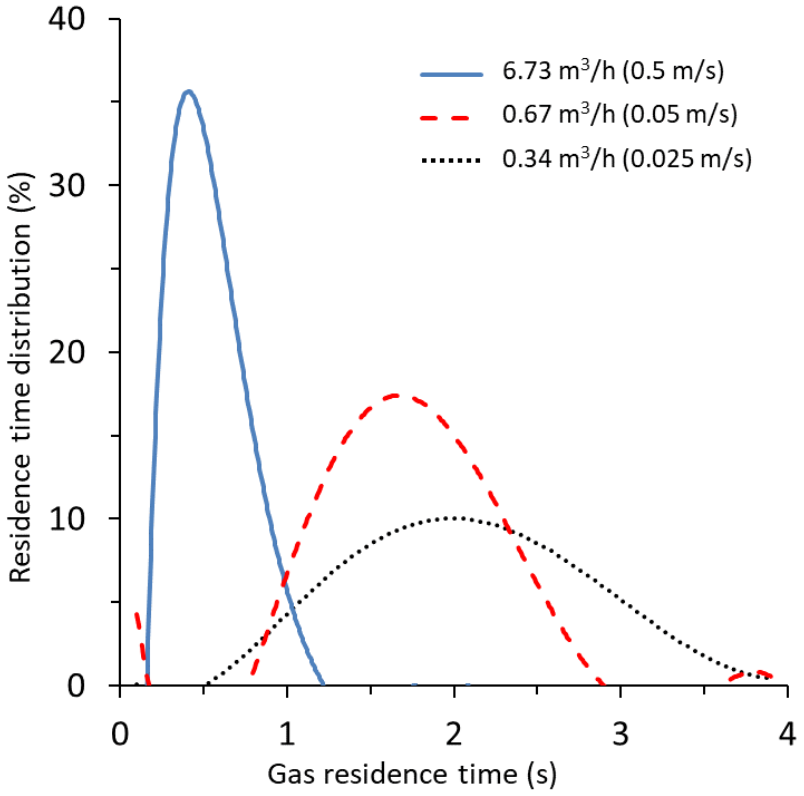

Fig. 8. Effect of the nitrogen flow rate (0.34−6.73 m^3/h) on the gas residence time.

In addition to affecting the gas residence time, the nitrogen flow rate also plays an important role in defining the biomass distribution (volume fraction), velocity and devlolatilization rate, as demonstrated in Fig. 9. A dramatic change in the biomass velocity and concentration takes place when the nitrogen flow rate is increased from 0.673 m^3/h to 6.73 m^3/h. Note that, at 6.73 m^3/h nitrogen flow, the estimated drag force exerted on the biomass is high, more than 3 times higher the particle weight force. At this condition, the biomass is packed below the gas exit pipe (see the third contour in Fig. 9a), while the velocity is excessively high in most of the upper part of the reactor (see the third contour in Fig. 9b). Obviously, this will have a negative impact on the mass and heat transfer rates at the core of the reactor due to the non-uniformity in flow structure. It is also clear from the contour in Fig. 9c that the devolatailization rate is close to zero in most of the upper part of the reactor.

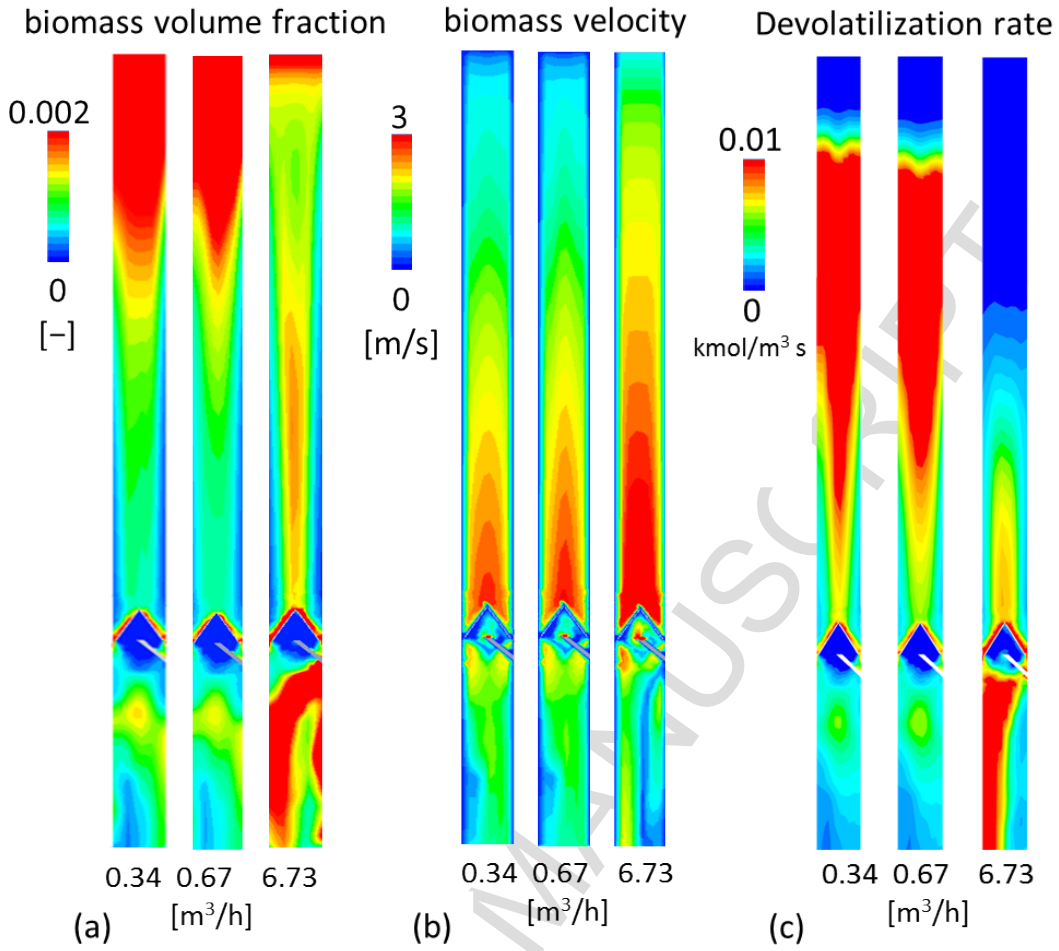

Fig. 9. Effect of the nitrogen flow rate (0.34−6.73 m^3/h) on (a) biomass volume fraction (b) biomass velocity (the biomass volume fraction is restricted to 0.002 to allow better visualization) and (c) on biomass devolatilization rate.

Finally, Fig. 10 shows the effect of nitrogen flow rate on the overall pyrolysis product yield. Operating at the nitrogen velocity of 0.05 m/s (0.67 $m^3\ h^{-1}$) appears to give high bio-oil yield (59.0 wt%). At the highest nitrogen flow rate of 0.5 m/s (6.73 $m^3\ h^{-1}$), the bio-oil and the NCG drop by 15% and 11%, respectively, which comes at the expense of increasing the char. This is due to insufficient biomass and gas residence times and the negative impact of this on the reactor temperature and overall flow hydrodynamics. As noted earlier in the introduction, various studies on free fall or downer reactors have discussed the optimum sweeping gas flow or velocity for maximum bio-oil yield (e.g. Gable [14]; Ellens [15]; Onay and Kockar [16]). However, generalization of such results for different reactors sizes and operating conditions is meaningless. It is of more relevance to use the relation between the sweeping gas drag force

and the particle weight force (F_d/W), since this is indirectly indicative of the relation between the sweeping gas flow, residence time and heat transfer rate for a particle undergoing pyrolysis in a downer reactor. In this study, the maximum bio-oil and NCG yield was found at F_d/W = 0.23.

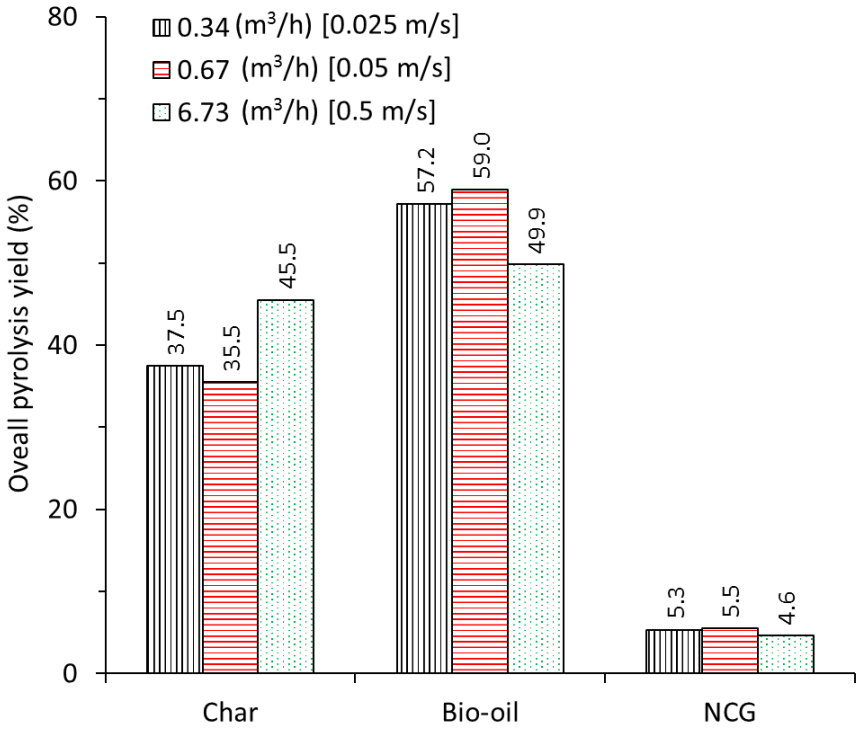

Fig. 10. Effect of the nitrogen flow rate (0.34−6.73 m³/h) on the distribution of the pyrolysis products.

6. Conclusions

Parameter sensitivity analysis of biomass fast pyrolysis in a downer reactor has been studied using a Eulerian-Eulerian CFD approach where the pyrolysis is considered to undergo one global step reaction. According to the predicted results, the following conclusions are made:

a) The pyrolysis temperature is the most effective parameter in the overall product yield and distribution. In this study, the temperature has been changed by increasing the heat carrier flow rate from 50 g/s up to 100 g/s. This has been found to increase considerably the bio-oil and NCG yields by 118% and 124%, respectively, at the expense of decreasing the bio-char yield.

b) The change in the biomass particle size within the range of 200−500 μm, has been

found to cause a negligible effect on the reactor hydrodynamics and overall product yield and distribution. The effect of the sand particle size, on the other hand, has been found to cause a major change in the reactor flow structure as well as in the products yield. The bio-oil and NCG yields both increased by around 30% when decreasing the particle size from 500 μm to 200 μm. This is mainly due to the increase in heat transfer surface area as the particle size decreases.

c) The nitrogen flow rate strongly affects the gas residence time. Excessive nitrogen flow, exerting a drag force higher than the single particle weigh ($F_d/W >> 1.0$), may result in shifting the gas residence time beyond the recommended range for fast pyrolysis (1−2 s). In this study, operating at a moderate gas flow of 0.67 m^3/h (0.05 m/s), which is calculated to correspond to F_d/W= 0.23, is found to produce the highest bio-oil and NCG yields. At this condition, the hydrodynamics and devolatilization rate appear to improve, with the latter rapidly taking place within the upper core section of the reactor.

d) The investigated parameters are interrelated; therefore, any optimization or extrapolation of the operating conditions for a targeted product (bio-oil, char or NCG) must be exercised with caution.

Acknowledgment: The authors thank The Leverhulme Trust (UK) for a research grant (RPG-410).

Notations

A_i	Interfacial area (m^2)
C_p	Specific heat (J $kg^{-1}K^{-1}$)
C_{vol}	Concentration of volatiles in biomass (mol m^{-3})
d_i	Diameter of solid phase i (m)
E	Activation energy (-)
$\vec{g}$	Gravity (m s^{-2})
h	Specific enthalpy (kJ kg^{-1})
h'	Heat transfer coefficient (w m^2 k^{-1})
$H(T)$	Enthalpy at temperature T (KJ/kg)
$\Delta H^{\circ}_{f,298}$	Heat of formation at temperature 298K (KJ/kg)
$\vec{J}_{i,g}$	Diffusion flux of species i (kg m^{-2} s^{-1})
k_m	Mass transfer coefficient (s^{-1})
L	Reactor length (m)
$\dot{m}$	Mass transfer rate (kg m^{-3} s^{-1})
Nu_{s_i}	Nusselt number of solid phase i (-)
P	Pressure (pa)
Pr	Prandtl number (-)
$\vec{q}$	Heat flux (w m^{-3})
Q_{gs_1}	Intensity of heat exchange between gas and solid (kJ m^{-3} s^{-1})
Q_{in}	Required thermal input for pyrolysis (Kw)
R	8.314 (J/mol K)
R_g,R_{s_i}	Interphase mass transfer term (kg m^{-3} s^{-1})
Re_{s_i}	Reynolds number of solid phase i (-)
r	Rate of pyrolysis reaction (mol m^{-3} s^{-1})
S	Source of enthalpy due to chemical reaction (kJ m^{-3} s^{-1})
T	Temperature (K)
t	Time (s)
$\vec{u}_g$,$\vec{u}_{s_i}$	Gas and solid velocity vectors, repectively (m s^{-1})
U_{mf}	Minimum fluidization velocity (m s^{-1})
U_p	Particle velocity (m s^{-1})
$Y_{i,g}$	Mass fraction

Greek symbols

α_g,α_{s_i}	Volume fraction of gas and solid phase i respectively (-)
β	Momentum exchange (drag) coefficient (kg m^{-3} s^{-1})
$\gamma_{\Theta_{s_i}}$	Collisional energy dissipation (kg m^{-1} s^{-3})
η	Separation efficiency (-)
Θ_{s_i}	Granular temperature of solid phase i (m^2 s^{-2})
$\kappa_{\Theta_{s_i}}$	Diffusion coefficient of granular energy (kg m^{-1} s^{-1})
λ_{s_i}	Particle bulk viscosity (kg m^{-1} s^{-1})
ρ_g ,ρ_{s_i}	Gas and solid densities, respectively (kg m^{-3})
τ	Solid residence time (s)
$\bar{\tau}$	Shear stress tensor (kg m^{-1} s^{-2})

654

655

656 **References**

[1] Lede, Jacques, Biomass Fast Pyrolysis Reactors: a Review of a few Scientific Challenges and of Related Recommended Research Topics. Oil & Gas Science and Technology– Rev. IFP Energies nouvelles, Vol. 68 (2013), No. 5, 801-814.

[2] A. V. Bridgwater, Review of fast pyrolysis of biomass and product upgrading, Biomass and Bioenergy, 38 (2012) 68-94.

[3] Yu, X., Makkawi, Y., Ocone, R., Berruti, F., Beriens, C., Huard, M., A CFD study of biomass pyrolysis in a downer reactor equipped with a novel gas-solid separator - I: hydrodynamic performance. Fuel Processing Technology (2014), 366-382.

[4] Zhu, J.-X., Yu, Z.-Q., Yin, Y., Grace, J. R., Issangya A., Cocurrent downflow circulating fluidized bed (downer) reactors − A state of the art review. The Can. J. of Chem Eng. (1995), Vol 73, Issue5, 662-677.

[5] Muktar Bashir, Yu, X., Hassan, M., Yassir Makkawi, Modelling and performance analysis of biomass fast pyrolysis in a solar-thermal reactor, ACS Sustainable Chem. Eng. (2017), 3795−3807.

[6] Elewuwa, F., Makkawi, Y., A computational model of hydrogen production by steam reforming of DME in a large-scale CFB reactor: Part II: Parametric analysis, International Journal of hydrogen production (2016), 19819-19828.

[7] Yu, X., Hassan, M., Ocone, R., Makkawi, Y., A CFD study of gas-soid separation in a downer pyrolysis reactor equipped with a novel gas-solid separator- II: Thermochemical performance and products, Fuel Processing Technology (2015), 51-63.

[8] Hassan, M and Makkawi, Y., A hydrodynamic model for biomass gasification in a circulating fluidized bed riser, Chemical Engineering and Processing- Process Intensification, Chemical Engineering & Processing: Process Intensification (2018), 148–161.

[9] Bridgwater, A. V., Renewable fuels and chemicals by thermal processing of biomass. Chem. Eng. J. (2003), 91, 87–102.

[10] Lin F., Waters C. L., Mallinson R. G., Lobban L. L., Bartley L. E., Relationships between biomass composition and liquid products formed via pyrolysis. Front. Energy Res. (2015), 3:45

693 [11] Yu, Q., et al., *Temperature impact on the formation of tar from biomass pyrolysis in a*
694 *free-fall reactor.* Journal of Analytical and Applied Pyrolysis (1997), 40-41, 481-489.
695
696 [12] Westerhof, R. J., Brilman, D. W., van Swaaij, W. P., Kersten, S. R., Effect of temperature in
697 fluidized bed fast pyrolysis of biomass: oil quality assessment in test units, Industrial & Engineering
698 Chemistry Research (2009), 49, 1160-1168.
699
700 [13] Gerçel, H. F., The production and evaluation of bio-oils from the pyrolysis of sunflower-oil
701 cake,Biomass and Bioenergy (2002), 23, 307-314
702
703 [14] Gable, Preston, The effect of process variables on pyrolysis in a freefall reactor. Graduate Theses
704 and Dissertations (2014).
705
706 [15] Ellens, C. J., Design, optimization and evaluation of a free-fall biomass fast pyrolysis reactor and
707 its products, Graduate Theses and Dissertations, Iowa State University (2009).
708
709 [16] Onay O. and Koçkar O. M., Pyrolysis of rapeseed in a free fall reactor for production of bio-oil,
710 Fuel (2006), 85, 1921-1928.
711
712 [17] Shen, J. Wang, X.-S., Garcia-Perez, M., Mourant, D., Rhodes M. J., Li, C.-Z., Effects of particle
713 size on the fast pyrolysis of oil mallee woody biomass, Fuel (2009), 88, 1810-1817.
714
715 [18] Liu, R., Shen, C., Wang, J., Liu, S., Effect of Particle Size of Corn Stalk Fast Pyrolysis on
716 Physicochemical Properties of Bio-Oil, Journal of Biobased Materials and Bioenergy (2010), 4, 391-
717 396.
718
719 [19] Uzun, B. B., Pütün, A. E., Pütün, E., Rapid pyrolysis of olive residue. 1. Effect of heat and mass
720 transfer limitations on product yields and bio-oil compositions, Energy & fuels (2007), 21, 1768-1776.
721
722 [20] Jahirul, M. J., Rasul, M. G., Chowdhury, A. A., Ashwath, N., Biofuels production through biomass
723 pyrolysis- a technological review, Energies (2012), 5, 4952-5001.
724
725 [21] Huard, M., An Investigation of a Novel Gas–Solid Separator for Downer Reactors, M. E. Sc. Thesis
726 The University of Western Ontario, London, Canada (2009).
727

728 [22] Huard, M., Berruti, F., Briens, C., Experimental Study of a Novel Fast Gas-Solid Separator for
729 Pyrolysis Reactors, International Journal of Chemical Reactor Engineering (2010), 8, 1542-6580.
730
731 [23] Boateng, A. and Mtui, P., CFD modeling of space-time evolution of fast pyrolysis products in a
732 bench-scale fluidized-bed reactor, Applied Thermal Engineering (2012), 33, 190-198.
733
734 [24] Pasangulapati, V., Devolatilization characteristics of cellulose, hemicellulose, lignin and the
735 selected biomass during thermochemical gasification: experiment and modeling studies. Thesis,
736 Oklahoma State University (2012).
737
738 [25] Boateng, A. A.; Daugaard, D. E.; Goldberg, N. M.; Hicks, K. B. Bench-scale fluidized-bed
739 pyrolysis of switchgrass for bio-oil production. Ind. Eng. Chem. Res. 2007, 46 (7), 1891−1897.
740
741 [26] ANSYS Fluent. Ansys fluent theory guide, version 15.0; Ansys Inc.: Cecil Township, PA.
742
743 [27] Vasquez, S. A. and Ivanov, V. A. "A Phase Coupled Method for Solving Multiphase
744 Problem on Unstructured Meshes," Fluids Engineering Division Summer Meeting, ASME,
745 Boston, 11-15 June 2000.
746
747 [28] Demirbas, Ayhan, Production and Characterization of Bio-Chars from Biomass via Pyrolysis,
748 Energy Sources, Part A: Recovery, Utilization, and Environmental Effects, Volume 28 (2006) - Issue 5
749
750 [29] Seebauer, V., Petek, J., Staudinger, G. Effects of particle size, heating rate and pressure
751 on measurement of pyrolysis kinetics by thermogravimetric analysis Author links open overlay
752 panel, Fuel (1997), Volume 76, Issue 13, 1277-1282.
753
754 [30] Septien, S., Valin, S., Dupont, C., Peyrot, M., Salvador, S., Effect of particle size and
755 temperature on woody biomass fast pyrolysis at high temperature (1000-1400 degrees C). Fuel
756 (2012), 97, 202-210.
757
758 [31] Makkawi, Y. and Wright, P. C., The void function and effective drag force for fluidized
759 beds. Chemical Engineering Science (2003), 58 (13), 2035-2051.
760
761 [32] Ghirelli, F., Hermansson, S., Thunman, H., Leckner, B., Reactor residence time analysis
762 with CFD, Progress in Computational Fluid Dynamics, (2006), 6 (4/5), 241−247.

763

764 [33] A.V. Bridgwater, G.V.C. Peacocke, Fast pyrolysis processes for biomass, Renewable &
765 Sustainable Energy Reviews (2000), 4, 1–73.

Highlights

- Parametric analysis of fast pyrolysis in a downer reactor has been carried out using CFD modeling.
- The pyrolysis temperature is the most effective parameter in the bio-oil yield.
- The size of the heat carrier (sand) affects the hydrodynamics and overall thermochemical conversion.
- The nitrogen flow rate strongly affects the gas residence time and devolatilization rate.